Supplement of

The impact of atmospheric motion on source-specific black carbon and the induced direct radiative effect over a river-valley region

Huikun Liu[1], Qiyuan Wang[1,2,4*], Suixin Liu[1,5], Bianhong Zhou[3], Yao Qu[1], Jie Tian[1], Ting Zhang[1], Yongming Han[1,2,4], Junji Cao[6,5*]

[1]State Key Laboratory of Loess and Quaternary Geology, Institute of Earth Environment, Chinese Academy of Sciences, Xi'an, 710061, China

[2]CAS Center for Excellence in Quaternary Science and Global Change, Xi'an, 710061, China

[3]Shaanxi Key Laboratory of Disaster Monitoring and Mechanism Simulation, College of Geography & Environment, Baoji University of Arts & Sciences, Baoji 721013, China

[4]Guanzhong Plain Ecological Environment Change and Comprehensive Treatment National Observation and Research Station, Xi'an 710061, China

[5]Shaanxi Key Laboratory of Atmospheric and Haze-fog Pollution Prevention, Xi'an 710061, China

[6]Institute of Atmospheric Physics, Chinese Academy of Sciences, Beijing 100029, China

[*]*Correspondence to*: Qiyuan Wang (wangqy@ieecas.cn) and Junji Cao (jjcao@mail.iap.ac.cn)

Table S1. The results of Bootstrap (BS) and displacement (DISP)

DISP Diagnostics:					
	Error Code:	0			
	%dQ:	-1.772433856			
	Swaps by Factor:	0	0	0	0
BS Mapping:					
	Base Factor 1	Base Factor 2	Base Factor 3	Base Factor 4	Unmapped
Boot Factor 1	49	0	0	1	0
Boot Factor 2	0	50	0	0	0
Boot Factor 3	0	0	50	0	0
Boot Factor 4	2	0	0	48	0

Table S2. The MAC and AAE derived from the positive matrix factorization model

	Diesel vehicular emissions	Coal combustion	Biomass burning	Fossil fuel combustion
MAC (m^2 g^{-1})	6.7	7.5	9.5	7.1
AAE	1.07	1.74	2.13	1.26

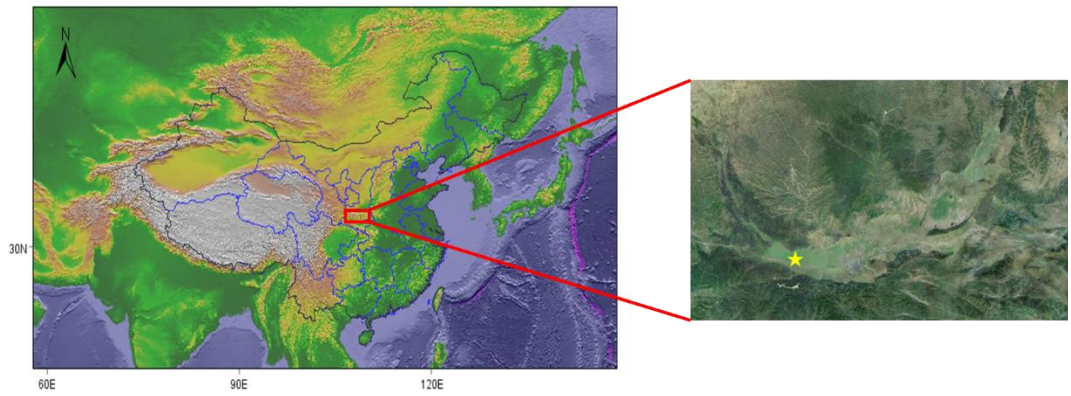

Figure S1. A map of the research site; the red box in the left figure represents Guanzhong Plain; the yellow star in the right figure represents the sampling site.

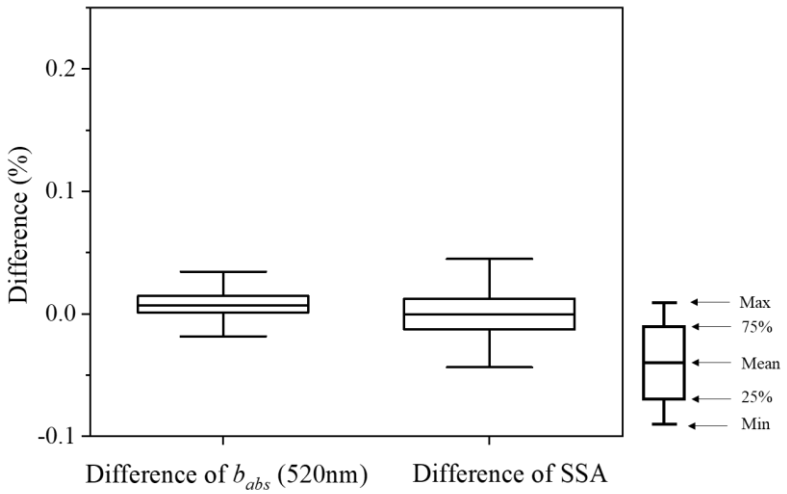

Figure S2. The difference between the modelled b_{abs}(500nm)/SSA and the observed b_{abs}(520nm)/SSA.

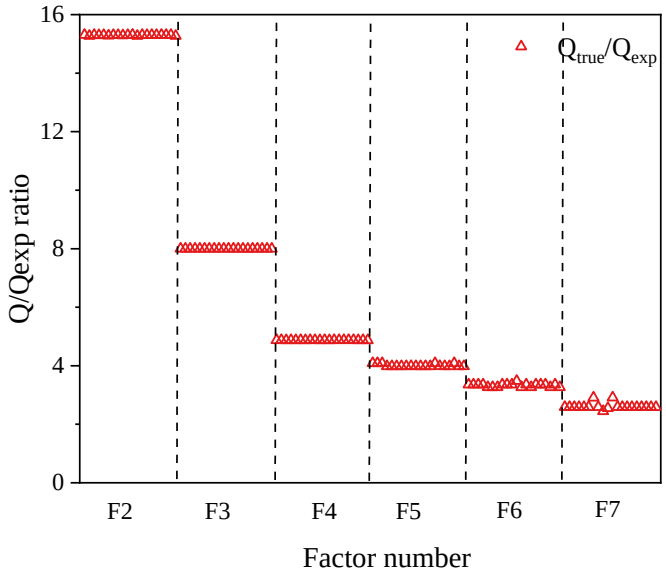

Figure S3. Variation of the ratio $Q_{true}/Q_{expected}$ for factor selection from 2 to 7 factors. The red triangles are the $Q_{true}/Q_{expected}$ values for each run for different factor solutions.

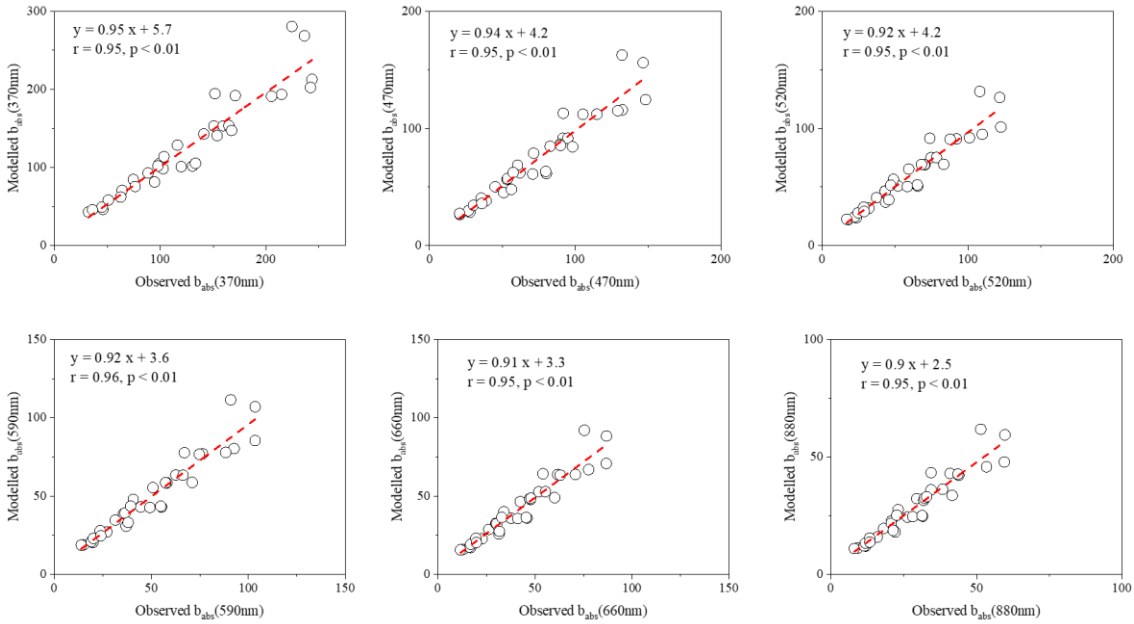

Figure S4. The linear relationship between the observed $b_{abs}(\lambda)$ and positive matrix factorization modelling b_{abs} (λ). λ includes 370nm, 470nm, 520nm, 590nm, 660nm and 880nm. The red line is a linear fitting line.

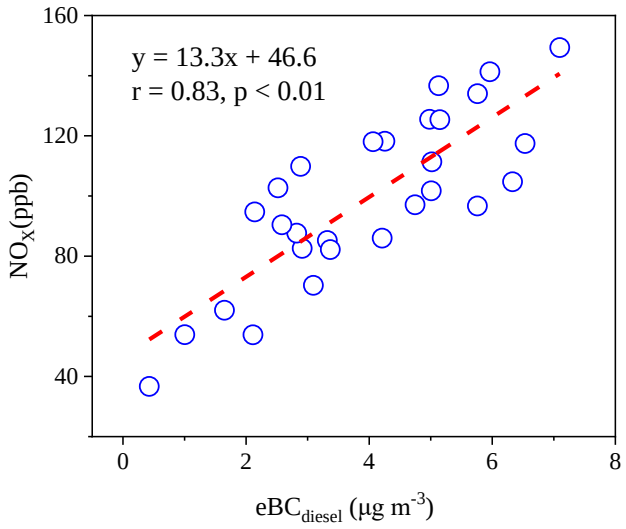

Figure S5. The correlation between NO_x and the eBC emitted from diesel vehicular emissions (eBC_{diesel}). The red line is a linear fitting line.

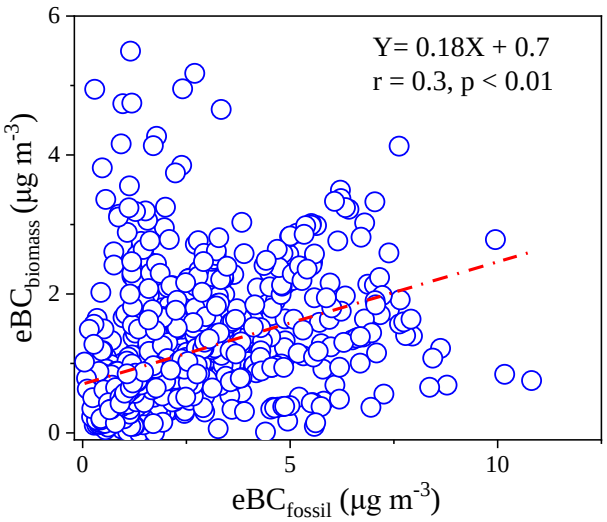

Figure S6. The correlation between eBC from biomass burning ($eBC_{biomass}$) and the eBC emitted from fossil fuel combustion (eBC_{fossil}). The red line is a linear fitting line.

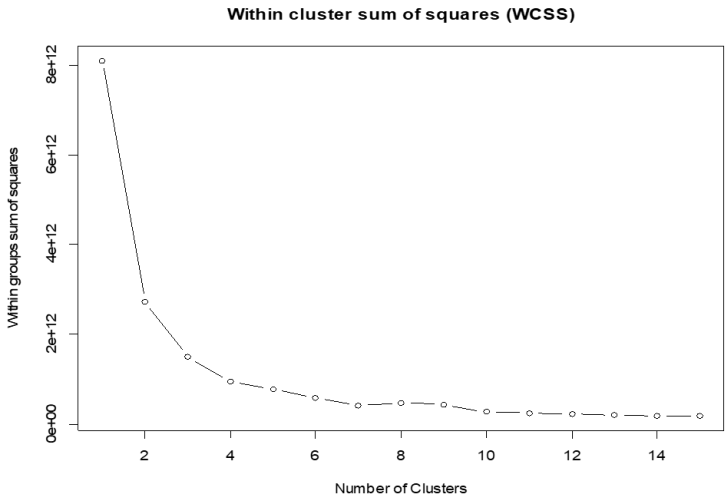

Figure S7. The result of K-means cluster method

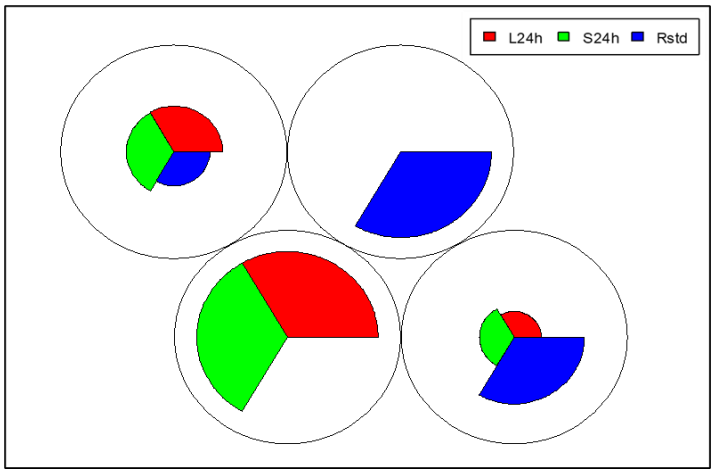

Figure S8. The result of the self-organizing map

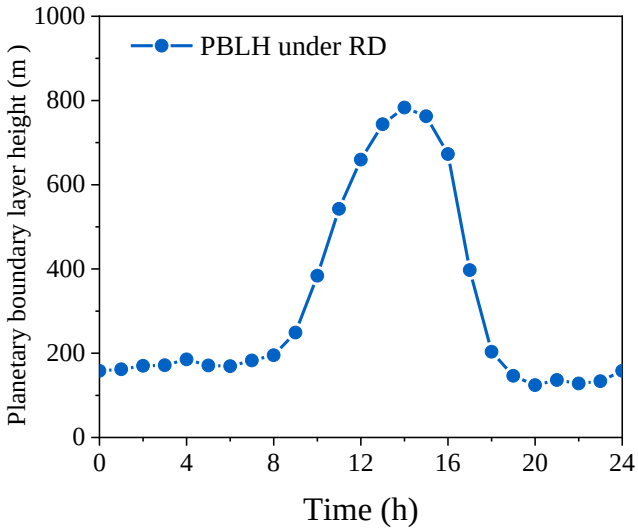

Figure S9. The diurnal variations of planetary boundary layer height (PBLH, m) under the dominance of regional scale of motion (RD)

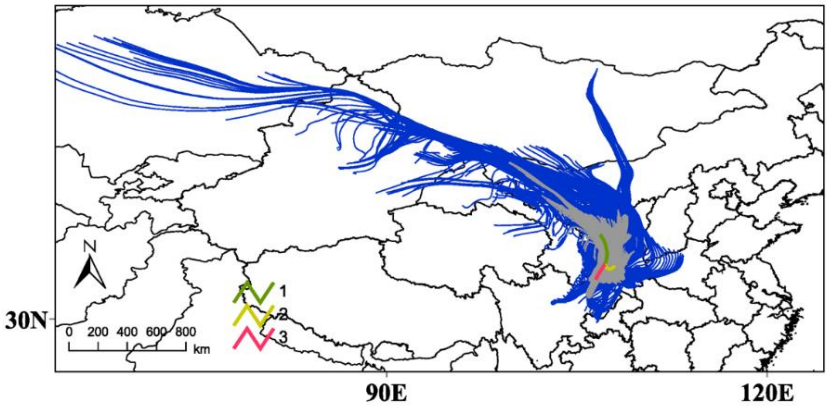

Figure S10. 24h-back trajectories (grey lines) and 72h-back trajectories (blue lines), and clusters at the sampling site 100 m above the ground. The green line represents Cluster No. 1, the yellow line represents Cluster No. 2, and the red line represents Cluster No. 3.